https://doi.org/10.2478/acph-2025-0019

Original research paper

Exploration of the chemical space of benzamide-based voltage-gated potassium channel $K_V1.3$ inhibitors

MARZIA FOIS[1,a]

ŠPELA PELCAR[1,a]

JOSHUA A. NASBURG[2]

HEIKE WULFF[2]

LUCIJA PETERLIN MAŠIČ[1,*]

TIHOMIR TOMAŠIČ[1,*]

[1] *University of Ljubljana, Faculty of Pharmacy, 1000 Ljubljana, Slovenia*

[2] *University of California, Davis, Department of Pharmacology, 451 Health Science Drive, Davis, CA 95616, USA*

[a] The authors contributed equally to this work.

* Correspondence; e-mails: lucija.peterlin@ffa.uni-lj.si; tihomir.tomasic@ffa.uni-lj.si

ABSTRACT

The voltage-gated potassium channel $K_V1.3$ is a key regulator of T-cell activation and a validated therapeutic target for autoimmune and inflammatory diseases. In this study, a ligand-based design strategy was employed to expand a library of benzamide-derived $K_V1.3$ inhibitors. Starting from a previously optimized thiophene-based inhibitor, structural modifications were introduced to the 2-methoxybenzamide moiety and the central tetrahydropyran or cyclohexane scaffold. A series of ketone, hydroxy, and carbamate derivatives was synthesized and evaluated for $K_V1.3$ inhibition using whole-cell patch-clamp electrophysiology. Structure–activity relationship analysis revealed that *cis*-isomers in the hydroxy series exhibited stronger activity

than their *trans* counterparts, with some analogs displaying submicromolar IC_{50} values. In the carbamate series, *trans*-isomers were generally more potent, with *trans*-**18** and *trans*-**16** achieving IC_{50} values of 122 nM and 166 nM, respectively. These results provide valuable insights into the design of $K_V1.3$ inhibitors and support further development of these compounds for immunomodulatory applications.

Keywords: $K_V1.3$, inhibitor, ion channel, ligand-based design, molecular modeling

Accepted May 30, 2025
Published online June 1, 2025

INTRODUCTION

Potassium channels are transmembrane proteins that facilitate the selective passage of potassium ions across the plasma membrane following their electrochemical gradient. These channels are classified into different families, with voltage-gated potassium channels (K_V) representing a major group. The $K_V1.x$ (Shaker) subfamily, the largest within this group, consists of eight members ($K_V1.1$–$K_V1.8$) (1, 2). $K_V1.3$ is widely expressed throughout the human body and plays a crucial role in numerous cellular processes. It is located in the plasma membrane, the inner mitochondrial membrane (mito$K_V1.3$), the nuclear membrane, and the membrane of the *cis*-Golgi apparatus (3). $K_V1.3$ expression has been identified in multiple cell types including neurons, osteoclasts, epithelial cells, and immune cells such T- and B-lymphocytes, macrophages and microglia, where it contributes to the regulation of membrane potential and calcium signaling (2).

Given the well-established role of T-cells in the pathogenesis of autoimmune diseases, $K_V1.3$ has emerged as an attractive therapeutic target. It is highly expressed in effector memory T (T_{EM}) cells, which mediate autoimmune disorders, as well as in other leukocytes involved in chronic inflammatory diseases, such as B-lymphocytes, macrophages, microglia, and dendritic cells. Inhibition of $K_V1.3$ has been shown to induce membrane depolarization, thereby preventing T-cell proliferation and cytokine production. Consequently, the development of selective $K_V1.3$ inhibitors that specifically target disease-inducing T_{EM} cells while preserving normal immune function could be beneficial in treating autoimmune and chronic inflammatory conditions, including psoriasis, multiple sclerosis, type 1 diabetes mellitus, atherosclerosis, asthma, and rheumatoid arthritis (4, 5).

K_V1.3 has also been identified as a promising molecular target for anticancer therapy due to its involvement in critical cellular processes, including proliferation, calcium signaling, cell volume regulation, adhesion, migration, apoptosis, and invasion (6). Although K_V1.3 is increasingly recognized as a tumor marker, a definitive pattern distinguishing its expression in cancerous versus healthy cells has not yet been established, as its levels appear to be influenced by the tumor type and disease stage (7). Nevertheless, aberrant K_V1.3 expression has been observed in breast, colon, and prostate tumors, as well as in smooth muscle and skeletal muscle cancers. It is also present in mature neoplastic B-cells in chronic lymphocytic leukemia, with a notable correlation between its expression and mitochondrial localization.[6] Potential therapeutic strategies for cancer treatment involve selectively inhibiting cancer cell proliferation or inducing apoptosis (8). Induction of apoptosis in cancer cells by K_V1.3 inhibition might be considered as an effective method to selectively kill cancer cells (9). Beyond its roles in immunity and oncology, K_V1.3 has been implicated in pathways regulating energy homeostasis and body weight, making it a potential target for obesity treatment (10).

One of the primary challenges in developing K_V1.3 inhibitors lies in the high sequence homology among K_V1.x family members, making it difficult to achieve potent and selective inhibition of K_V1.3. Several K_V1.3 inhibitors have been designed to specifically target K_V1.3 in the plasma membrane. Among them, the psoralen derivative PAP-1 (**1**, Fig. 1) is currently the most potent (IC_{50} = 2 nM) and selective (*i.e.* 23-fold over K_V1.5) small-molecule K_V1.3 inhibitor (11). The antimycobacterial drug clofazimine (**2**, Fig. 1) is another well-characterized K_V1.3 inhibitor (IC_{50} = 300 nM), displaying tenfold selectivity over K_V1.1, K_V1.2, K_V1.5, and K_V3.1 (12). Another important K_V1.3 inhibitor, a benzamide derivative known as PAC (**3**, Fig. 1), was identified through a high-throughput screening campaign. It exhibited an IC_{50} of 200 nM but lacked selectivity among K_V1.x family members. *In vitro* functional assays demonstrated that this compound reversibly inhibits calcium-dependent T-cell activation and suppresses IL-2 production in a concentration-dependent manner without inducing cytotoxicity or affecting calcium-independent T-cell stimulation pathways (13).

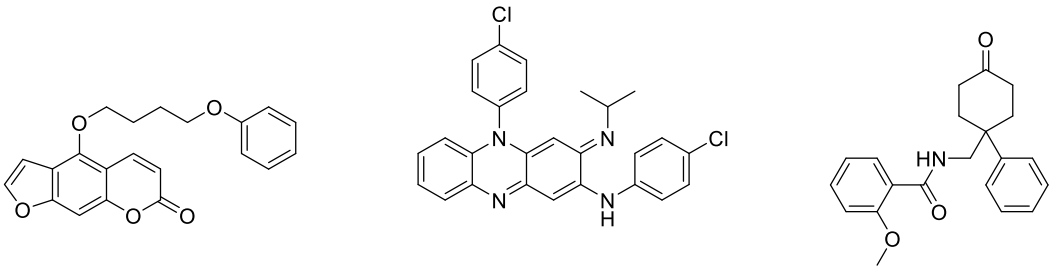

Fig. 1. Structures of known representative $K_V1.3$ inhibitors PAP-1 (**1**), clofazimine (**2**) and PAC (**3**).

Since the binding site of benzamide-based $K_V1.3$ inhibitors remains unidentified, we employed a ligand-based drug design strategy, utilizing a 3D similarity search of previously reported benzamide inhibitors. This approach led to the discovery of a novel thiophene-based compound **A**, which demonstrated selectivity for $K_V1.3$ channels (14). Further structural modifications of compound **A** resulted in the development of the 3-thiophene-based inhibitor **B** (Fig. 2), which demonstrated an IC_{50} of 470 nM and an 18-fold selectivity over related $K_V1.x$ family channels in *Xenopus laevis* oocytes (15). Additional optimization led to compound **C**, which inhibited $K_V1.3$-mediated currents in activated human T-lymphocytes with an IC_{50} value of 26.1 nM (16). In this work, we further investigate the structure-activity relationship (SAR) of this series by extensively modifying the 2-methoxybenzamide moiety of the inhibitor while retaining the 3-thienyl group at position 4 of the core tetrahydropyran or cyclohexane ring (Fig. 2).

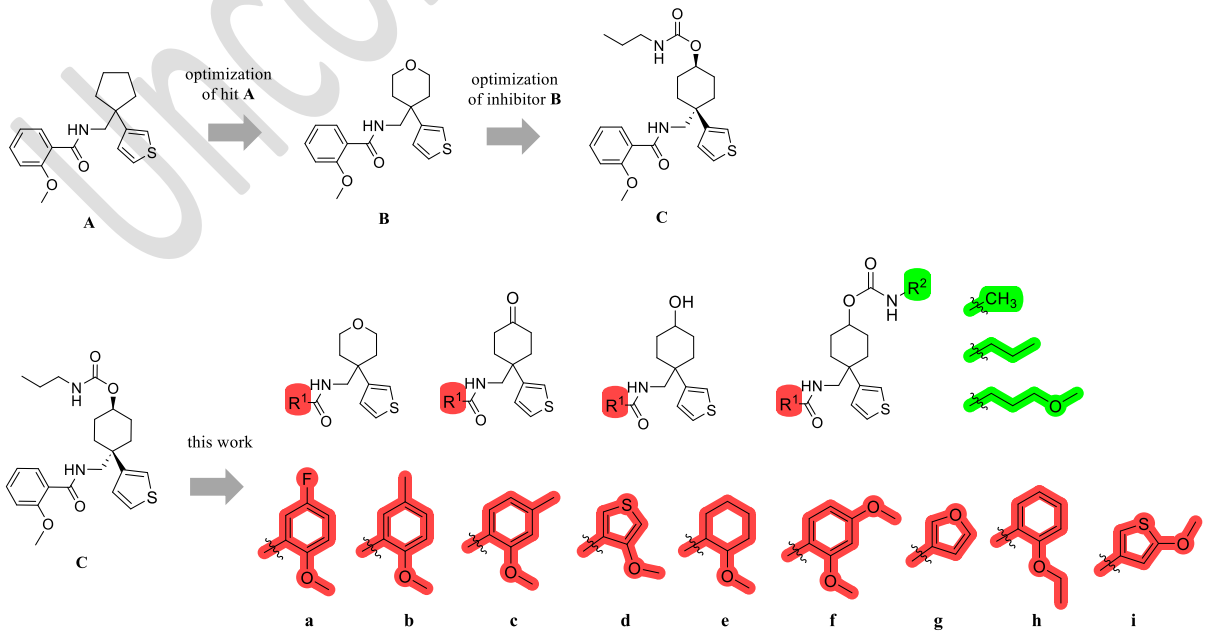

Fig. 2. Optimization of $K_V1.3$ inhibitor **A**, identified by virtual screening, to more potent analogs **B** and **C**, and further structure-activity relationship investigation in this work.

EXPERIMENTAL

Chemistry – General

The reagents and solvents used were obtained from commercial sources (*i.e.*, Acros Organics, Sigma-Aldrich, TCI Europe, Merck, Carlo Erba, Apollo Scientific) and were used as provided. Analytical thin-layer chromatography (TLC) was performed on silica gel aluminum sheets (60 F_{254}, 0.20 mm; Merck). Flash column chromatography was performed on silica gel 60 (particle size 0.040–0.063 mm, Merck). ^{1}H NMR and ^{13}C spectra were recorded at 400 and 100 MHz, respectively, on a Bruker Avance III NMR spectrometer (Bruker, MA, USA) at 295 K. The chemical shifts (δ) are reported in ppm and are referenced to the deuterated solvent used. HRMS measurements were performed on a LC-MS/MS system (Q Executive Plus; Thermo Scientific, MA, USA). Mass spectrometry measurements were performed on an Expression CMS^{L} mass spectrometer (Advion, USA). Analytical reversed-phase UPLC analyses were performed using a modular system (Thermo Scientific Dionex UltiMate 3000 modular system; Thermo Fisher Scientific Inc., USA). Method: Waters Acquity UPLC® HSS C18 SB column (2.1 × 50 mm, 1.8 µm), t = 40 °C; injection volume = 5 µL; flow rate = 0.4 mL min^{-1}; detector λ = 254 nm; mobile phase A (0.1 % trifluoroacetic acid (TFA) [v/v] in water), mobile phase B acetonitrile (MeCN). Gradient: 0–2 min, 10 % B; 2–10 min, 10 %–90 % B; 10–12 min, 90 % B. Purities of the tested compounds were established to be ≥95 % at 254 nm, as determined by UPLC. The syntheses of the compounds are illustrated in Schemes 1 and 2, experimental procedures and characterization data are provided in the Supporting information.

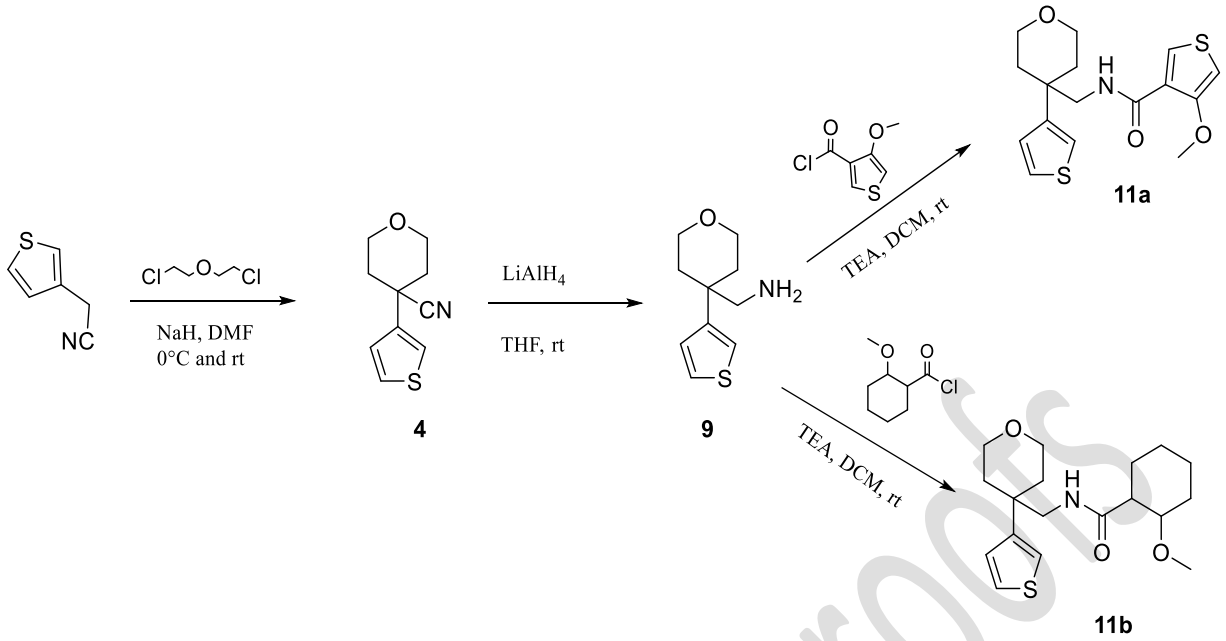

Scheme 1. Synthesis of the target compounds **11a** and **11b**.

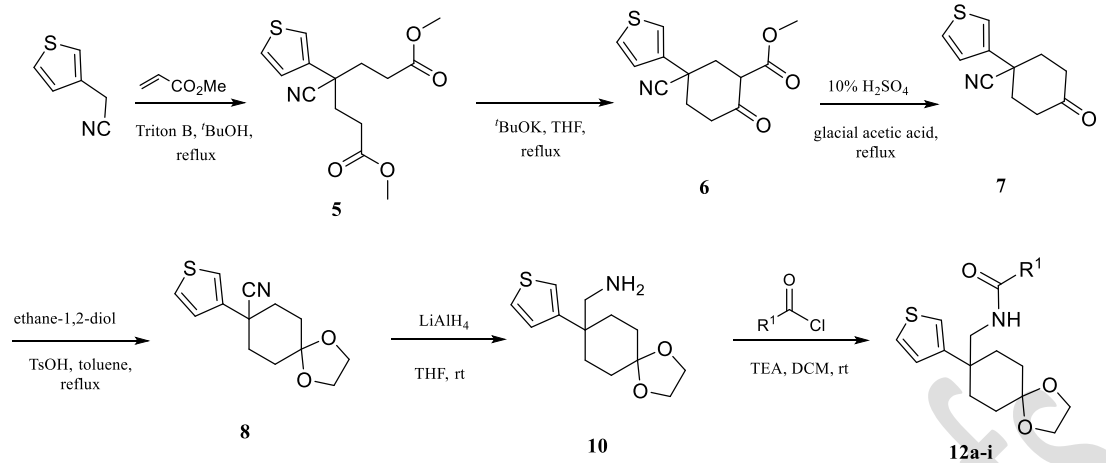

12a R^1 = 5-fluoro-2-methoxybenzene
12b R^1 = 2-methoxy-5-methylbenzene
12c R^1 = 2-methoxy-4-methylbenzene
12d R^1= 3-methoxythiophene
12e R^1 = 2-methoxycyclohexane
12f R^1= 2,4-dimethoxybenzene
12g R^1= furan
12h R^1= 2-ethoxybenzene
12i R^1 = 2-methoxythiopene

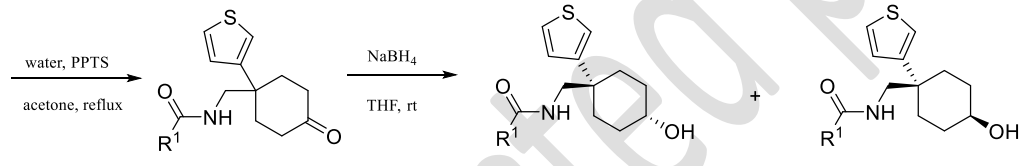

13a R^1 = 5-fluoro-2-methoxybenzene
13b R^1 = 2-methoxy-5-methylbenzene
13c R^1 = 2-methoxy-4-methylbenzene
13d R^1 = 3-methoxythiophene
13e R^1 = 2-methoxycyclohexane
13f R^1 = 2,4-dimethoxybenzene
13g R^1 = furan
13h R^1 = 2-ethoxybenzene
13i R^1 = 2-methoxythiopene

trans-**14a** R^1 = 5-fluoro-2-methoxybenzene
trans-**14b** R^1 = 2-methoxy-5-methylbenzene
trans-**14c** R^1 = 2-methoxy-4-methylbenzene
trans-**14 d** R^1 = 3-methoxythiophene
trans-**14g** R^1 = furan
trans-**14i** R^1 = 2-methoxythiphene

cis-**14a** R^1 = 5-fluoro-2-methoxybenzene
cis-**14b** R^1 = 2-methoxy-5-methylbenzene
cis-**14c** R^1 = 2-methoxy-4-methylbenzene
cis-**14d** R^1 = 3-methoxythiophene
cis-**14g** R^1 = furan
cis-**14i** R^1 = 2-methoxythiophene

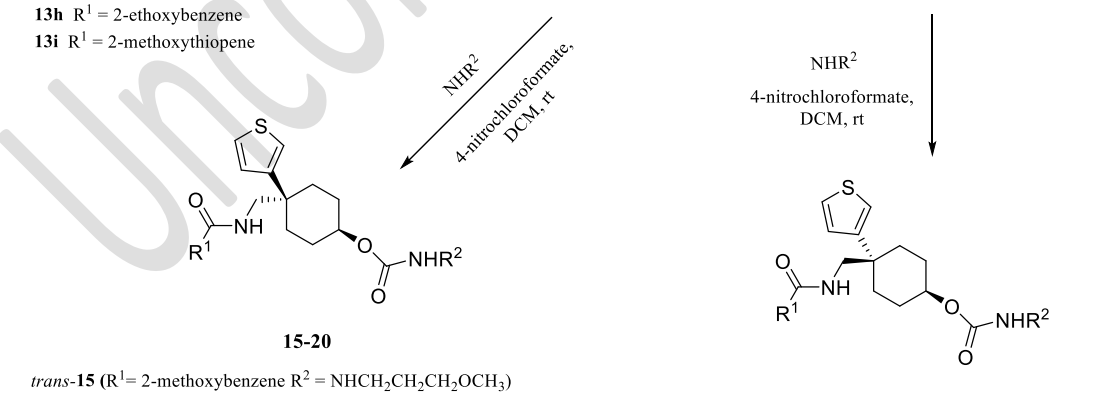

trans-**15** (R^1= 2-methoxybenzene R^2 = $NHCH_2CH_2CH_2OCH_3$)
trans-**16** (R^1 = 3-methoxythiophene R^2 = $NHCH_2CH_2CH_3$)
trans-**17** (R^1 = 2-methoxy-4-methylbenzene R^2 = $NHCH_2CH_2CH_3$)
trans-**18** (R^1 = 5-fluoro-2-methoxybenzene R^2 =$NHCH_2CH_2CH_3$)
trans-**19** (R^1 = furan R^2 = $NHCH_3$)
trans-**20** (R^1 = furan R^2 =$NHCH_2CH_2CH_3$)

cis-**21** (R^1 = 2-methoxy-4-methylbenzene R^2 = $NHCH_2CH_2CH_3$)

Scheme 2. Synthesis of the target compounds **13a-i**, *trans*-**14a-d**, *trans*-**14g**, *trans*-**14i**, *cis*-**14a-d**, *cis*-**14g**, *cis*-**14i**, *trans*-**15-20** and *cis*-**21.**

Patch-clamp electrophysiology

Mouse L929 fibroblasts stably expression mK_V1.3, were a gift from Dr. K. George Chandy (University of California, Irvine, USA). All experiments were conducted with an EPC-10 amplifier (HEKA, Lambrecht/Pfalz, Germany) in the whole-cell configuration with a holding potential of -80 mV. Pipette resistances averaged around 2.5 MΩ. Compound solutions were prepared fresh in Na^+ Ringer from 10 mM stock solutions in DMSO directly before the experiments. For current measurements, we used an internal pipette solution containing 160 mM KF, 2 mM $MgCl_2$, 10 mM HEPES, and 10 mM EGTA, with a pH of 7.2 and an osmolarity of ~ 300 mOsm. Sodium Ringer was used as an external solution containing the following: 160 mM NaCl, 4.5 mM KCl, 2 mM $CaCl_2$, 1 mM $MgCl_2$, and 10 mM HEPES, with a pH of 7.4 and an osmolarity of ~ 300 mOsm. Currents were elicited with a 200-ms voltage step to + 40 mV, followed by 45 seconds of holding at a resting membrane potential of –80 mV. A use-dependence protocol, whereby cells were pulsed to 40 mV every 1 second, was used prior to the step protocol for compound to ensure that channel kinetics were as expected. If currents exceeded 2 nA 60–80 % series resistance compensation was used. Concentration dependent current inhibition as measured as reduction of area under the current curve was fitted with the Hill equation using GraphPad Prism 8 (GraphPad Software, USA). All data points represent at least 3 independent experiments and are presented as mean ± standard deviation (SD). IC_{50} values are reported with 95 % confidence intervals (CI).

RESULT AND DISCUSSION

Chemistry

Based on our previously published compounds (15, 16), we further investigated the SAR for K_V1.3 inhibition (Fig. 2). We synthesized compounds **11a** and **11b**, in which the 3-thiophene and tetrahydropyran moieties were retained, while the 2-methoxyphenyl group of compound **B** was replaced with either a 2-methoxycyclohexyl or 3-methoxythiophenyl moiety, respectively. Next, the tetrahydropyran ring was substituted with a cyclohexane ring bearing keto, hydroxy, or carbamate groups. Compounds **13a–i** contain a ketone at the 4-position of the cyclohexane ring and feature various modifications of the 2-methoxybenzamide moiety. Reduction of the ketone in compounds **13a–h** produced the corresponding hydroxy analogs: *trans*-**14a–d**, *cis*-**14a–d**, *trans*-**14g**, *cis*-**14g**, *trans*-**14i**, and *cis*-**14i**. These hydroxy compounds were then further

modified to generate methylcarbamate-, propylcarbamate-, and 3-methoxypropylcarbamate-containing derivatives **15–21**. All hydroxy- and carbamate-substituted compounds were obtained as diastereomeric mixtures, which were subsequently separated into their *cis*- and *trans*-isomers using column chromatography. The synthetic routes for these new compounds are outlined in Schemes 1 and 2.

In Scheme 1, thiophene-3-acetonitrile was reacted with 1-chloro-2-(2-chloroethoxy)ethane in the presence of sodium hydride (NaH, 60 % dispersion in mineral oil) under an argon atmosphere at room temperature, yielding the intermediate 4-(thiophen-3-yl)tetrahydro-2*H*-pyran-4-carbonitrile (**4**). The nitrile group was subsequently reduced using lithium aluminum hydride ($LiAlH_4$) in tetrahydrofuran (THF) to produce the primary amine **9**. This amine was then reacted with either 4-methoxythiophene-3-carbonyl chloride or 2-methoxycyclohexane-1-carbonyl chloride to afford the final compounds **11a** and **11b**.

For the synthesis of cyclohexane-based analogs (Scheme 2), thiophene-3-acetonitrile was refluxed in *tert*-butanol and subjected to a double Michael addition in the presence of methyl acrylate and benzyl trimethylammonium hydroxide (Triton B), yielding the diester intermediate **5**. In the following step, compound **5** was deprotonated using potassium *tert*-butoxide and underwent Dieckmann condensation to form the 4-heteroaryl-4-cyano-2-carbomethoxycyclohexanone derivative **6**. The 2-carboxymethyl group was then removed by heating at 100 °C in a mixture of 10 % sulfuric acid and glacial acetic acid, producing 4-oxo-1-(thiophen-3-yl)cyclohexane-1-carbonitrile (**7**). The ketone group of **7** was protected with ethylene glycol, forming compound **8**. Subsequent reduction of the nitrile group using $LiAlH_4$ in THF provided the primary amine **10**, which was then acylated with various acyl chlorides to produce intermediates **12a-i**. Deprotection of the ketone yielded compounds **13a-i**. Selective reduction of the ketone group in **13a-i** using sodium borohydride ($NaBH_4$) produced diastereomeric mixtures of alcohols **14a-i**, which were separated into their *cis*- and *trans*-isomers by column chromatography. The resulting hydroxy analogs were reacted with 4-nitrochloroformates to form 4-nitrophenyl carbonate intermediates, which were subsequently treated with various primary amines to yield novel carbamate derivatives *trans*-**15**, *trans*-**16**, *trans*-**17**, *trans*-**18**, *trans*-**19**, *trans*-**20**, and *cis*-**21**.

Determination of K_V1.3 inhibition

To expand the library of 2-methoxybenzamides, a series of new K_V1.3 inhibitors was synthetized and evaluated for their inhibitory activity at 1 μM and 10 μM using whole-cell

patch-clamp electrophysiology (Tables 1-3). Replacement of the 2-methoxyphenyl moiety in compound **B** (Fig. 2) with a 2-methoxycyclohexyl, as in **11b**, resulted in loss of inhibitory activity, while compound **11a** with 3-methoxythiophen-4-yl group showed full inhibition of $K_V1.3$ at 10 μM (Table I). Within the ketone series, compound **13a**, featuring a 5-fluoro substituent on the 2-methoxyphenyl ring, exhibited the highest potency, achieving 49 % inhibition at 1 μM and complete block at 10 μM. Substitution with either a 4-methyl (**13c**) or 4-methoxy (**13f**) group on the 2-methoxyphenyl ring was better tolerated than a 5-methyl substituent (**13b**), which showed reduced activity. Strong inhibition was also observed when the 2-methoxyphenyl group was replaced with a 3-methoxythiophen-4-yl (**13d**) or a 2-ethoxyphenyl group (**13h**). In contrast, compounds **13e** (bearing a methoxycyclohexyl group) and **13g** (with a furan-3-yl substituent) only weakly inhibited $K_V1.3$ at 10 μM (Table I).

*Table I. $K_V1.3$ inhibitory activity of new analogs **11a**, **11b** and **13a-h**, manually patch-clamped to determine the percentage of inhibition at 1 μM and 10 μM (n = 3)*

Compound	Structure	Average % block at 1 μM	Average % block at 10 μM
11a	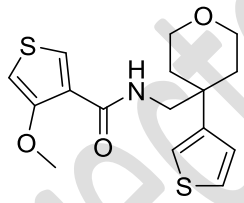	60 %	100 %
11b	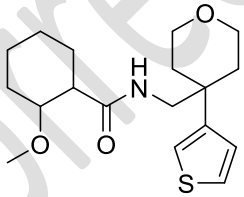	0 %	22 %
13a	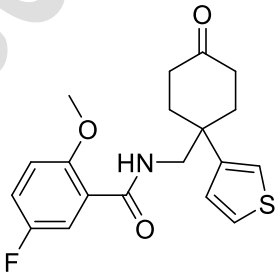	49 %	100 %
13b	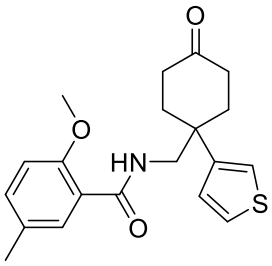	9 %	63 %

13c	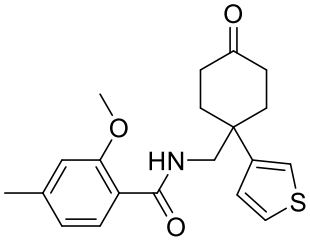	32 %	89 %
13d	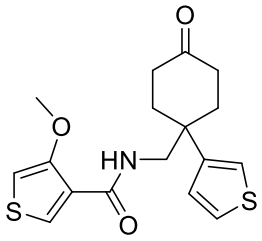	25 %	92 %
13e	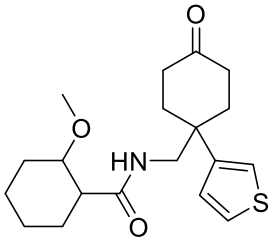	4 %	25 %
13f	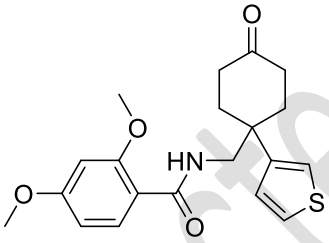	27 %	85 %
13g	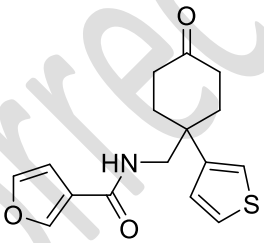	0 %	20 %
13h	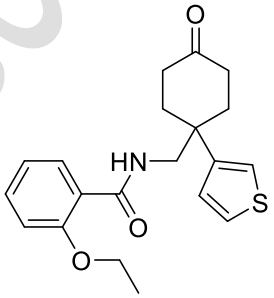	29 %	88 %

In the hydroxy series (**14a-d,g,i**), an SAR pattern similar to that observed for the ketones (**13a–h**) was evident. Notably, the *cis*-isomers consistently exhibited more potent $K_V1.3$ inhibition than their *trans* counterparts, regardless of the substitution on the 2-methoxyphenyl ring. Among the hydroxy derivatives, the most potent compounds were *cis*-

14c, *cis*-**14d**, and *cis*-**14i**, bearing 4-methyl-2-methoxyphenyl, 3-methoxythiophen-4-yl, and 2-methoxythiophen-3-yl substituents, respectively. Each of these compounds achieved complete $K_V1.3$ inhibition at 1 μM (Table II). In the carbamate series (Table III), the 3-methoxypropyl analog of compound **C** (*trans*-**15**) also demonstrated full $K_V1.3$ inhibition at 1 μM. Consistent with findings from our previous study,[16] the *trans*-carbamates generally exhibited stronger inhibitory activity than their *cis* counterparts. For example, *trans*-**17** inhibited $K_V1.3$ by 87 % at 1 μM, whereas *cis*-**21** showed only 21 % inhibition at the same concentration. Other potent inhibitors included the propylcarbamates *trans*-**16** and *trans*-**18**, analogs of **14d** and **14a**, respectively, both of which showed complete inhibition at 1 μM (Table III). Based on this preliminary screening, the most promising compounds, *cis*-**14c**, *cis*-**14d**, *cis*-**14i**, *trans*-**15**, *trans*-**16**, *trans*-**17**, and *trans*-**18**, were selected for further evaluation in concentration-response experiments (Table IV).

*Table II. $K_V1.3$ inhibitory activity of new analogs **14a-d,g,i**, manually patch-clamped to determine the percentage of inhibition at 1 μM and 10 μM (n = 3)*

Compound	Structure	Average % block at 1 μM	Average % block at 10 μM
trans-**14a**	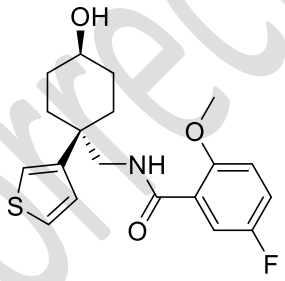	31 %	80 %
cis-**14a**	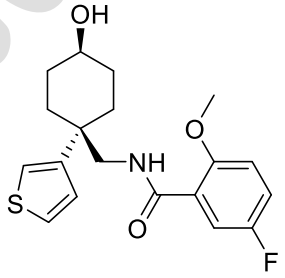	84 %	100 %
trans-**14b**	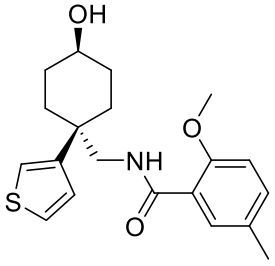	11 %	40 %

cis-**14b**	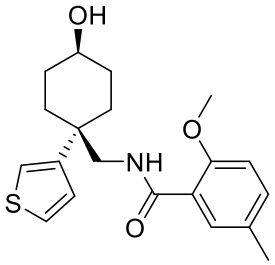	49 %	100 %
trans-**14c**	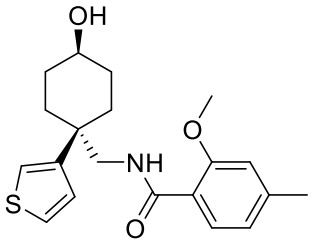	0 %	32 %
cis-**14c**	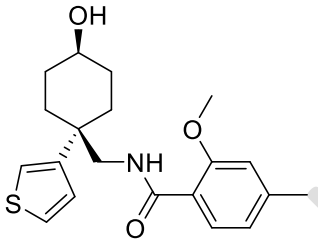	100 %	n.t.
trans-**14d**	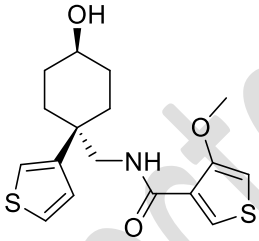	12 %	52 %
cis-**14d**	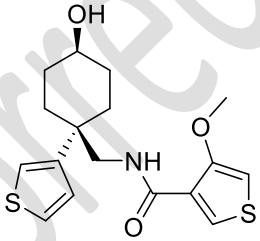	100 %	n.t.
trans-**14g**	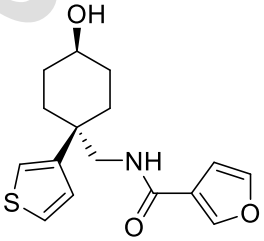	0 %	0 %
cis-**14g**	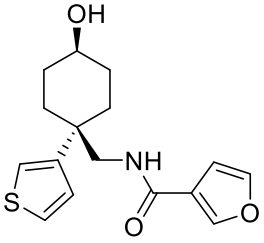	10 %	40 %

trans-**14i**	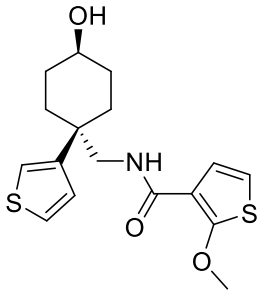	19 %	77 %
cis-**14i**	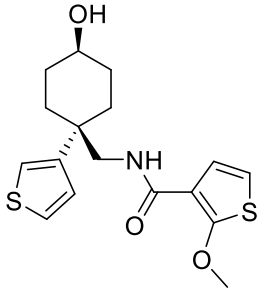	100 %	n.t.

*Table III. $K_V1.3$ inhibitory activity of new analogs **15-21**, manually patch-clamped to determine the percentage of inhibition at 1 μM and 10 μM (n =3). n.t. = not tested*

Compd.	Structure	Average % block at 1 μM	Average % block at 10 μM
trans-**15**	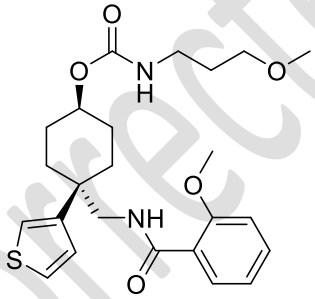	100 %	n.t.
trans-**16**	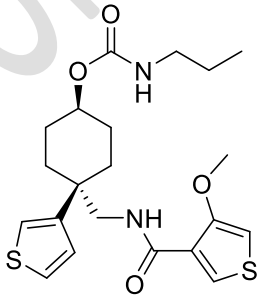	100 %	n.t.

trans-**17**	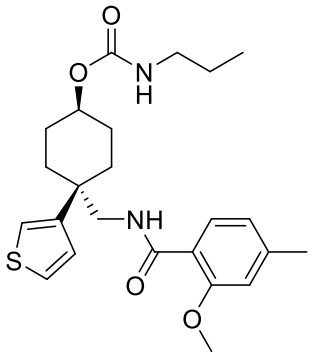	87 %	n.t.
trans-**18**	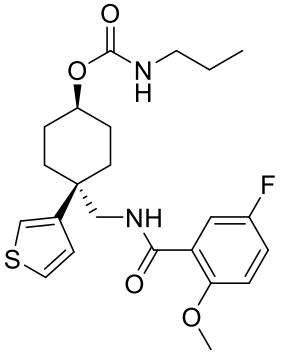	100 %	n.t.
trans-**19**	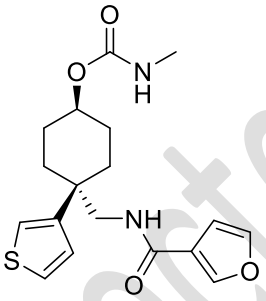	7 %	66 %
trans-**20**	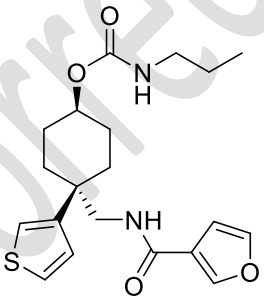	0 %	21 %
cis-**21**	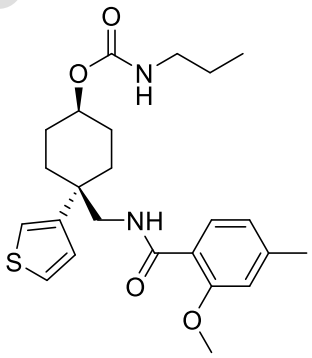	21 %	83 %

The potency of compounds *cis*-**14c**, *cis*-**14d**, and *cis*-**14i** was assessed by determining their IC_{50} values for $K_V1.3$ inhibition and compared to the reference compounds *cis*-**D** (IC_{50} =

226 nM) and *trans*-**D** (IC_{50} = 2.2 μM). Among the tested compounds, *cis*-**14i** showed the highest potency, with an IC_{50} of 326 nM, followed closely by *cis*-**14d** (IC_{50} = 346 nM) and *cis*-**14c** (IC_{50} = 505 nM). Although all three compounds displayed submicromolar IC_{50} values, they were less potent than *cis*-**D**. The potency of compounds *trans*-**15**, *trans*-**16**, *trans*-**17**, and *trans*-**18** was compared to the parent compound *trans*-**C** (IC_{50} = 0.23 μM). Among these, *trans*-**18** exhibited the highest potency, with an IC_{50} of 122 nM, followed by *trans*-**16** with an IC_{50} of 166 nM. While both compounds were less potent than *trans*-**C**, they still retained significant inhibitory activity. *trans*-**15** and *trans*-**17** were less potent than *trans*-**16** and *trans*-**18**, though their inhibitory potency remained within the submicromolar range. These results suggest that the 2-methoxyphenyl ring, as present in compound *trans*-**C**, represents an optimal substituent for $K_V1.3$ inhibition at this position. However, small modifications, such as those present in *trans*-**16** and *trans*-**18**, are well tolerated in maintaining strong inhibitory potency.

Table IV. IC_{50} *values determined on* $K_V1.3$ *channels*

Compd.	Structure	*IC*$_{50}$
cis-**14c**	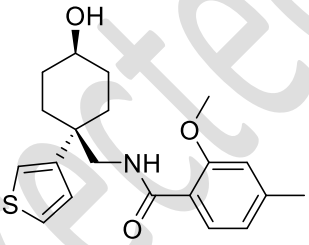	505 nM (95 CI: 445-561 nM)
cis-**14d**	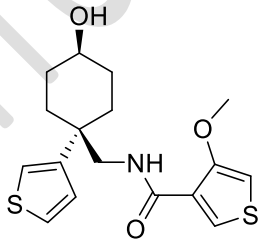	346 nM (95 CI: 317-377 nM)
cis-**14i**	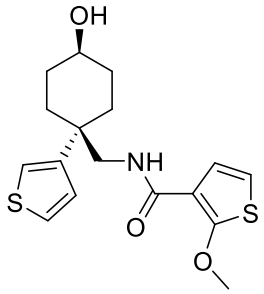	326 nM (95 CI: 298-357 nM)

trans-**15**	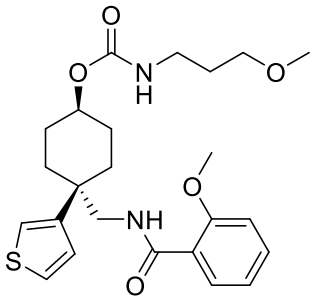	342 nM (95 CI: 319-367 nM)
trans-**16**	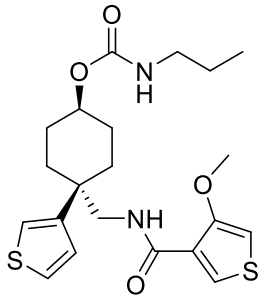	166 nM (95 CI: 154-179 nM)
trans-**17**	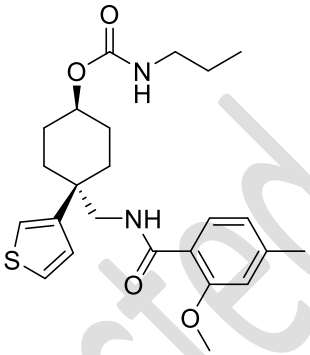	438 nM (95 CI: 411-466 nM)
trans-**18**	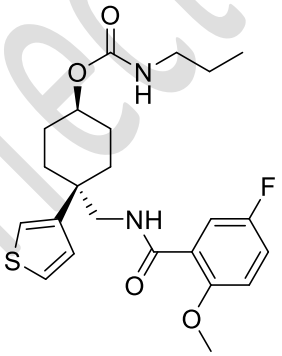	122 nM (95 CI: 102-144 nM)
trans-**C**	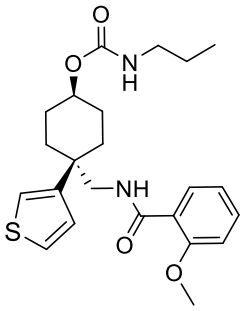	74 nM (95 CI: 65-84 nM)

cis-**D**	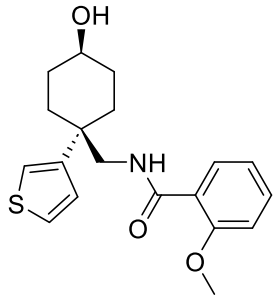	234 nM (95 CI: 220-242 nM)
trans-**D**	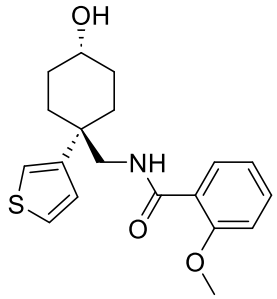	2.6 µM (95 CI: 2.0 – 3.2 µM)

CONCLUSION

In this study, a ligand-based design approach was used for the optimization of novel thiophene-based $K_V1.3$ inhibitors, building on previously reported benzamide scaffold. Structural modifications focused on the 2-methoxybenzamide moiety and the core tetrahydropyran or cyclohexane ring, while retaining the 3-thienyl group, enabled the identification of several potent inhibitors. Structure–activity relationship analysis revealed that *cis*-isomers in the hydroxy series consistently exhibited stronger $K_V1.3$ inhibition than their *trans* counterparts, with *cis*-**14i**, *cis*-**14d**, and *cis*-**14c** emerging as the most effective (IC_{50} = 326–505 nM). In the carbamate series, *trans*-isomers showed superior activity, with *trans*-**18** and *trans*-**16** achieving IC_{50} values of 122 nM and 166 nM, respectively. While none of the new compounds outperformed the most potent reference inhibitors, several analogs exhibited submicromolar potency. These findings provide valuable insights into the SAR of $K_V1.3$ inhibitors and highlight promising candidates for further development.

Notes

The authors declare no competing financial interest.

Acknowledgment. – This research was funded by Slovenian Research Agency (ARIS) grant numbers J7-4635 (MitoCan) and P1-0208. J.A.N. was supported by a National Institute of General Medical Sciences funded Pharmacology Training Program [T32GM099608].

Authors contributions. – The manuscript was written through contributions of all authors. all authors have given approval to the final version of the manuscript.

REFERENCES

(1) Yellen, G. The Voltage-Gated Potassium Channels and Their Relatives. *Nature* **419**(6902) (2002) 35–42; https://doi.org/10.1038/nature00978.
(2) Serrano-Albarrás, A.; Estadella, I.; Cirera-Rocosa, S.; Navarro-Pérez, M.; Felipe, A. Kv1.3: A Multifunctional Channel with Many Pathological Implications. *Expert Opin. Ther. Targets* **22**(2) (2018) 101–105; https://doi.org/10.1080/14728222.2017.1420170.
(3) Pérez-García, M. T.; Cidad, P.; López-López, J. R. The Secret Life of Ion Channels: Kv1.3 Potassium Channels and Proliferation. *Am. J. Physiol.-Cell Physiol.* **314**(1) (2018) C27–C42; https://doi.org/10.1152/ajpcell.00136.2017.
(4) Wulff, H.; Pennington, M. Targeting Effector Memory T-Cells with Kv1.3 Blockers. *Curr. Opin. Drug Discov. Devel.* **10**(4) (2007) 438–445.
(5) Chandy, K. G.; Norton, R. S. Peptide Blockers of K v 1.3 Channels in T Cells as Therapeutics for Autoimmune Disease. *Curr. Opin. Chem. Biol.* **38** (2017) 97–107; https://doi.org/10.1016/j.cbpa.2017.02.015.
(6) Comes, N.; Serrano-Albarrás, A.; Capera, J.; Serrano-Novillo, C.; Condom, E.; Ramón Y Cajal, S.; Ferreres, J. C.; Felipe, A. Involvement of Potassium Channels in the Progression of Cancer to a More Malignant Phenotype. *Biochim. Biophys. Acta BBA - Biomembr.* **1848**(10) (2015) 2477–2492; https://doi.org/10.1016/j.bbamem.2014.12.008.
(7) Comes, N.; Bielanska, J.; Vallejo-Gracia, A.; Serrano-Albarrás, A.; Marruecos, L.; Gómez, D.; Soler, C.; Condom, E.; Ramón Y Cajal, S.; Hernández-Losa, J.; Ferreres, J. C.; Felipe, A. The Voltage-Dependent K+ Channels Kv1.3 and Kv1.5 in Human Cancer. *Front. Physiol.* **4** (2013) 283 (13 pages). https://doi.org/10.3389/fphys.2013.00283.
(8) Serrano-Novillo, C.; Capera, J.; Colomer-Molera, M.; Condom, E.; Ferreres, J.; Felipe, A. Implication of Voltage-Gated Potassium Channels in Neoplastic Cell Proliferation. *Cancers* **11**(3) (2019) 287 (17 pages); https://doi.org/10.3390/cancers11030287.
(9) Teisseyre, A.; Gąsiorowska, J.; Michalak, K. Voltage-Gated Ptassium Channels Kv1.3 - Potentially New Molecular Target in Cancer Diagnostics and Therapy. *Adv. Clin. Exp. Med.* **24**(3) (2015) 517–524; https://doi.org/10.17219/acem/22339.
(10) Pérez-Verdaguer, M.; Capera, J.; Serrano-Novillo, C.; Estadella, I.; Sastre, D.; Felipe, A. The Voltage-Gated Potassium Channel Kv1.3 Is a Promising Multitherapeutic Target against Human Pathologies. *Expert Opin. Ther. Targets* **20**(5) (2016) 577–591; https://doi.org/10.1517/14728222.2016.1112792.
(11) Schmitz, A.; Sankaranarayanan, A.; Azam, P.; Schmidt-Lassen, K.; Homerick, D.; Hänsel, W.; Wulff, H. Design of PAP-1, a Selective Small Molecule Kv1.3 Blocker, for

the Suppression of Effector Memory T Cells in Autoimmune Diseases. *Mol. Pharmacol.* **68**(5) (2005) 1254–1270; https://doi.org/10.1124/mol.105.015669.

(12) Ren, Y. R.; Pan, F.; Parvez, S.; Fleig, A.; Chong, C. R.; Xu, J.; Dang, Y.; Zhang, J.; Jiang, H.; Penner, R.; Liu, J. O. Clofazimine Inhibits Human Kv1.3 Potassium Channel by Perturbing Calcium Oscillation in T Lymphocytes. *PLoS one* **3**(12) (2008) e4009 (11 pages); https://doi.org/10.1371/journal.pone.0004009.

(13) Schmalhofer, W. A.; Bao, J.; McManus, O. B.; Green, B.; Matyskiela, M.; Wunderler, D.; Bugianesi, R. M.; Felix, J. P.; Hanner, M.; Linde-Arias, A.-R.; Ponte, C. G.; Velasco, L.; Koo, G.; Staruch, M. J.; Miao, S.; Parsons, W. H.; Rupprecht, K.; Slaughter, R. S.; Kaczorowski, G. J.; Garcia, M. L. Identification of a New Class of Inhibitors of the Voltage-Gated Potassium Channel, K_v 1.3, with Immunosuppressant Properties. *Biochemistry* **41**(24) (2002) 7781–7794; https://doi.org/10.1021/bi025722c.

(14) Hendrickx, L. A.; Dobričić, V.; Toplak, Ž.; Peigneur, S.; Mašič, L. P.; Tomašič, T.; Tytgat, J. Design and Characterization of a Novel Structural Class of Kv1.3 Inhibitors. *Bioorg. Chem.* **98** (2020) 103746 (9 pages). https://doi.org/10.1016/j.bioorg.2020.103746.

(15) Gubič, Š.; Hendrickx, L. A.; Shi, X.; Toplak, Ž.; Možina, Š.; Theemsche, K. M. V.; Pinheiro-Junior, E. L.; Peigneur, S.; Labro, A. J.; Pardo, L. A.; Tytgat, J.; Tomašič, T.; Mašič, L. P. Design of New Potent and Selective Thiophene-Based K_V1.3 Inhibitors and Their Potential for Anticancer Activity. *Cancers* **14**(11) (2022) 2595 (20 pages); https://doi.org/10.3390/cancers14112595.

(16) Gubič, Š.; Montalbano, A.; Sala, C.; Becchetti, A.; Hendrickx, L. A.; Van Theemsche, K. M.; Pinheiro-Junior, E. L.; Altadonna, G. C.; Peigneur, S.; Ilaš, J.; Labro, A. J.; Pardo, L. A.; Tytgat, J.; Tomašič, T.; Arcangeli, A.; Peterlin Mašič, L. Immunosuppressive Effects of New Thiophene-Based K_V1.3 Inhibitors. *Eur. J. Med. Chem.* **259** (2023) 115561 (17 pages); https://doi.org/10.1016/j.ejmech.2023.115561.